IEEE Access
Multidisciplinary | Rapid Review | Open Access Journal

Received June 12, 2019, accepted June 16, 2019, date of publication June 19, 2019, date of current version July 3, 2019.

Digital Object Identifier 10.1109/ACCESS.2019.2923661

Analysis of Mutual Couple Effect of UHF RFID Antenna for the Internet of Things Environment

GUOLONG SHI, YIGANG HE, BAIQIANG YIN, LEI ZUO, PEILIANG SHE, WENBO ZENG, AND FARHAN ALI

Institute of Electrical and Automation Engineering, Hefei University of Technology, Hefei 230000, China

Corresponding author: Yigang He (yigang_he@126.com)

This work was supported in part by the National Natural Science Foundation of China under Grant 51577046, in part by the State Key Program of National Natural Science Foundation of China under Grant 51637004, in part by the National Key Research and Development Plan "important scientific instruments and equipment development" under Grant 2016YFF0102200, and in part by the Equipment Research Project in Advance under Grant 41402040301.

ABSTRACT Asset management was a common RFID-based Internet-of-Things (IoT) application scene. RFID tags in the equipment warehouse were usually large, and the communication between the reader and the tag was prone to data collision problems, which affected the recognition efficiency of the device. In practical applications, due to the structural characteristics of the micro-strip UHF RFID tag antenna, the traditional inter-coupling impedance expression had large errors and insufficient accuracy in predicting the mutual coupling effect, such as system frequency shift. In this paper, the 3D initialization model of the tag was used to indirectly extract the electrical parameter values by the ANSYS HFSS software. At the same time, the dual-tag was taken as an example to derive the transimpedance expression between the dense tags to extract the corresponding coupling parameters. Finally, various tag-intensive scenarios in the actual environment were tested and the derivation formula was verified, and the dual-tag UHF RFID near-field frequency shift affected by the environmental factors, such as relative position, attachment, and the stacking method, was discussed. The mutual coupling effect on the minimum transmit power of the reader antenna was also studied. The experimental results showed that the average error of the formula calculated by this method was significantly smaller than that of the traditional formula. When the tag spacing was less than 30 mm, the derived mutual impedance expression was applied to the frequency shift calculation error range (1.6–7.3 MHz). For dense tag systems, the error was less than 9.8% when the number of tags was greater than 7, and the prediction accuracy was higher than the superposition method. The research results provided a theoretical and practical basis for the rapid identification and location of power assets during the dense RFID tag environment.

INDEX TERMS UHF RFID, Internet of Things, power asset management, frequency shift, mutual couple effect, mutual impedance.

I. INTRODUCTION

Internet of Things (IOT) connects a large number of information-aware devices through various access technologies for information exchange and communication, enabling intelligent identification, location, tracking, monitoring and management for smart homes, personal privacy, traditional industry, intelligent monitoring, engineering control and other fields [1]–[3]. IOT consists of five layers: sensing layer, access layer, network layer, support layer and application layer. The relationship between the layers is shown in Figure 1. The key technologies of IOT mainly include sensing and identification technologies, network communication technologies, data fusion technologies, cloud computing technologies, nanotechnology, and smart technologies. How to extract multiple data information through the sensing layer is one of the key issues that IOT needs to be solved. Among them, RFID is an important technology of the sensing layer, it is a non-contact automatic identification technology which can automatically recognizes target objects and acquires relevant data through radio frequency signals. The identification process can work in various harsh environments without manual intervention [4].

With the rapid development of national economy, the power industry has become one of the pillar industries.

The associate editor coordinating the review of this manuscript and approving it for publication was Vyasa Sai.

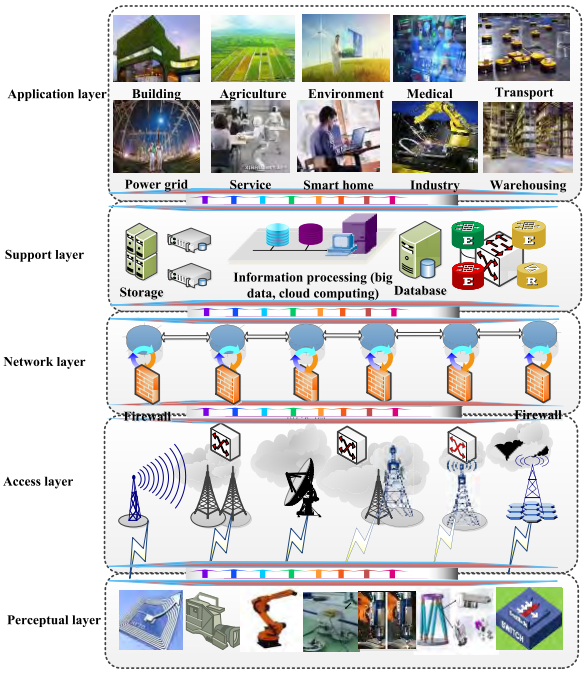

FIGURE 1. The relationship between the IOT layers.

Asset management is a common RFID-based IOT application scene. The asset management of power supply enterprises includes the management of the stock and distribution status of fixed assets, as well as the maintenance and management of the operating status of assets. As the update of equipment assets is fast, the level of asset management directly affects the operation and development of the enterprise [5]. The fixed asset management has always been a weak link in the management of power companies for a long time. The importance of automatic identification technology in enterprise informationization management has become more and more recognized and valued. ''Electronic ID card'' through RFID tags can realize stricter and more standardized tracking management of various assets. The asset physical management system that forms traceability information throughout the life of the asset provides accurate information support for the asset life management analysis. Through advanced identification and assistance, the inventory process is optimized to make the inventory more accurate, faster, and efficient. With the maturity of RFID technology, asset management is no longer limited to single-tag identification, and multiple tags are used at the same time [6]–[8]. Multiple tags exist in the range recognizable by the reader means that multiple tags will be read at the same time. The electromagnetic interference among tag antennas will impact the energy transmission efficiency, system recognition rate and working frequency [9], [10].

With the maturity of UHF RFID technology [11]–[13], near-field communication applications are no longer dominated by high frequency (HF) tags. It is widely expected that UHF RFID tags will dominate the Near Field (NF) application market in the next few decades [14]. On the other hand, the research of close-range communication between passive RFID tags [15] and wireless power transfer between tags [16] have opened up new application prospects in the UHF band. For example, Xiao *et al.* [17] proposed a comprehensive RFID localization system by attaching two RFID tags to one object, which can conveniently estimate positions of reader antennas and accurately locate and track RFID tags during complex environments. Wang and his co-workers [18] presented a device-free detection technology through wall that adopts passive RFID tags to perceive the absence or presence of moving persons and identify motion directions of a moving target. However, for the UHF RFID application, there are still many problems to be solved, such as the mutual impedance generated by densely placed tags, which may lead to problems such as reduced energy transmission efficiency and frequency shift [19]. The UHF RFID near-field has tangential, radial electric and magnetic field components corresponding to magnetic field (inductive) coupling and electric field (capacitor) coupling. Since the UHF near-field is mainly used in the identification of single products, it is often necessary to identify some tags attached to the surrounding environment, and the magnetic field is highly resistant to liquid environments. Therefore, the near-field antenna of the UHF RFID system is more magnetically coupled. In the case of densely placed tags, there is also a magnetic field coupling between the tags, which has an important impact on the RFID system. Zuo *et al.* [20] derived the expression of mutual impedance between tags under dense conditions, and analyzed the influence of mutual effects on the system. However, they only analyzed the interference tag which was located in the radiation far-field area of the working tag antenna, and the tag-intensive placement of the induction near-field area was not considered. When any dual-tag is in the near field region of each other, the gain of the tag will change qualitatively and the model is no longer applicable. Peng *et al.* [21], [22] studied the tags based on the inductive coupling principle, the density of the tag antenna and the frequency shift characteristics of the antenna self-impedance when densely placed in the UHF RFID sensing near-field region were also discussed. The tag antennas studied in the above literature were specific and cannot further analyze the mutual coupling effects of the system by affecting the environmental factors of the mutual impedance between tags.

Sunny *et al.* [23] detected the corrosion degree of metal objects by using the frequency shift caused by the coupling effect of metal on the tag. Han *et al.* [24] proposed a new anti-intrusion system detection method based on the influence of the coupling effect between the dual-tag on the RFID system. However, the above literature failed to fundamentally analyze the root cause of system frequency shift. For the frequency shift problem in dense tag system, a dense tag coupling circuit model was constructed to quantitatively analyze the cause of system frequency shift, but the theoretical results cannot be tested and analyzed [25]. The cross-resistance expression between dense tags was derived from the perspective of energy transfer, and the effects of mutual coupling effect

between dense tags on tag performance, such as antenna radiation efficiency and antenna gain were analyzed [26]. The frequency shift characteristics of the tag were studied from the perspective that the mutual coupling between the dense tags changed the structural parameters of the tag antenna [27]. A design method of tag antenna mutual impedance to overcome system mutual coupling effect in dense tag system was proposed by Peng *et al.* [22]. Zhu *et al.* [28] analyzed the influence of metal environment on the performance of tag antennas in HF band RFID systems, and proposed the concept of omnidirectional tags. Qing *et al.* [29] analyzed the influence of metal plate on the working frequency of tags, and proposed the research method of anti-metal tags applied in smart shelves to improve the detection accuracy of the system. The above literature only analyzes the performance changes of the tags in the dense tag RFID system when they were mutually coupled, the performance changes of the entire RFID system was not involved.

Specifically, the technical contributions of our paper can be concluded as follows:

First: this paper studied the mutual impedance expression between the tag antennas combined with transformer model, the inductively coupled tags were densely placed in the UHF RFID sensing near-field region from the perspective of wireless energy transmission.

Second: the inductive coupling type tag J41 was used for example, the transimpedance expression was verified by simulation and experiment. Then the indirect extraction parameters were modeled, and the derivation formula was compared with the traditional formula, and the mutual impedance value between the tags was introduced into the resonance frequency shift calculation of the tag.

Third: under an actual dense tags environment, system performance under vertical, parallel and tilt placements scenarios was tested. Finally, through the mutual impedance analysis, the influencing factors of frequency shift caused by the near-field mutual coupling effect were explored.

The rest of our paper was organized as follows. Experiment equipment included RFID tags, test instruments and experimental scenarios were introduced in Section. II. Section. III described related theoretical derivation of the proposed system. Coupling coefficient extraction, frequency shift analysis was discussed in detail in Section. IV. Finally, Section. V concluded the whole paper.

II. EXPERIMENT EQUIPMENT

A. TAG AND ITS PARAMETER EXTRACTION

UHF RFID near-field tags included traditional dipole tags, ring tags and T-type matching dipole tags, et.al. In this paper, the inductive coupling ultra-wideband ring tag named Impinj J41 was used for experiment. The specific parameters of Impinj J41 were shown in Table 1.

Due to the structural characteristics of the micro-strip tag antenna, this paper indirectly extracted its electrical parameter values by establishing a 3D initialization model for

TABLE 1. The specific parameters of Impinj J41.

Product name	Impinj J41 (Button)
Protocol	ISO18000-C
Product Size	Diameter: 12 mm
Chip	Monza 4D, 4E, 4QT
Working frequency	860~960 MHz
EPC capacity	128 bit
User data	512 bit
Material	Aluminum etching
Inlay life	100,000 readings and writes
Working distance	0.1-0.5 m
Application Scenes	Access control electronic ticket card, drug, asset management, close-range application

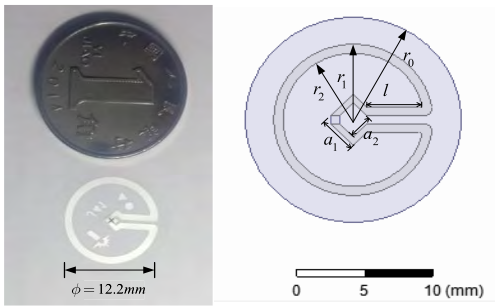

FIGURE 2. RFID Tag and its size.

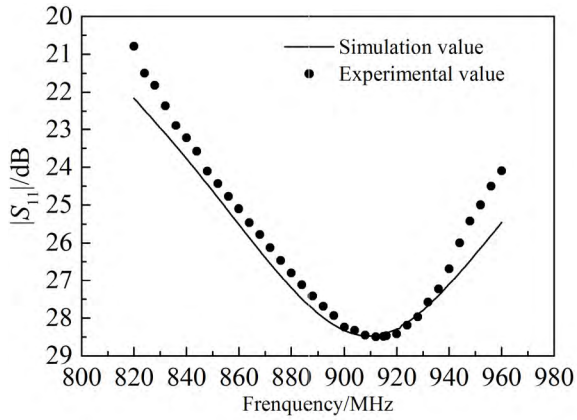

FIGURE 3. Return loss performance of tag J41.

the tags in ANSYS HFSS 16.0 (Finite Element Analysis Software in Electromagnetic Fields) software, as shown in Figure 2. The modeling of the tags involved Boolean operations, the solution type: mode drive; port excitation method was wave port excitation; frequency range: 820~960 MHz, scanning frequency: 5 MHz; in order to improve simulation speed, fast sweep mode was selected, model length resolution rate (MRL): 200 mil. The antenna was a planar coil, and the tag model parameters were shown in Table 2, where h was the thickness of the tag substrate and the matrix was the ideal conductor (PET: $\varepsilon_r = 3.0$, $\tan\theta = 0.02$).

From the simulation results, the impedance of the tag antenna $Z_{tl} = (10.2039 + j143.3921)\ \Omega$, as known from the J41 Datasheet, the parallel resistance of the chip Monza 4E was 2.48 pF (915 MHz), the load of the tag impedance

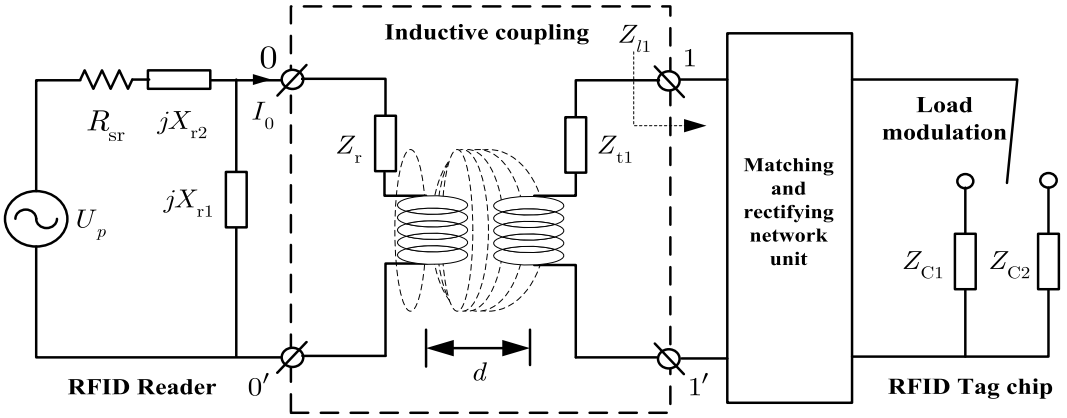

FIGURE 4. UHF RFID near-field magnetic field coupling circuit model.

TABLE 2. Tag parameters (parameters change slightly).

h	r_0	r_1	r_2	a_1	a_2	l
0.05	7.5	6.1	5.5	2.8	1.4	4.5

Note: (Unit: mm)

$Z_{l1} = (11\text{-}j143)\ \Omega$, it can be considered that the established tag model basically achieved the requirements of conjugate impedance matching. The return loss test analysis of the tagged object was carried out by the Agilent network analyzer, the test result compared with the simulated value was shown in Figure 3. The results showed that the performance of the simulation model was similar to the physical object. This paper established a simulation model to obtain the electrical value of the tag.

B. UHF RFID NEAR-FIELD LINK MODEL

The UHF RFID near-field system adopted transformer-type inductive coupling principles [15], as shown in Figure 4. The reader antenna was considered to be its primary coil and the tag antenna was considered to be its secondary coil. For an ordinary near-field antenna, the system was effective as long as the distance between the coils satisfied: $d < 0.16\ \lambda$ (about 5 cm), while the distance was not being able to meet practical needs. At present, many near-field readers can increase their effective reading distance to more than a dozen centimeters or even further by using a segmented loop antenna and so on [16]. Inductive coupling existed between the reader antenna and the tag antenna during the reader antenna identification range, moreover, the tag antennas also have inductive coupling with each other when the space among tag antennas was less than a few centimeters.

R_{sr} was the reader power supply resistance (usually 50 Ω); Z_r was the reader antenna impedance. In order to achieve the maximum power transmission between the reader power supply and the load, the antenna impedance matching network should be set. X_{r1} and X_{r2} were the reactive components of the L-type reader antenna impedance. Z_{t1} was the impedance of the tag antenna; Z_{l1} was the port 11' impedance, including the impedance of the matching network, the rectifying unit and the chip load. When the reader impedance matching coefficient $\rho = 1$, and $R_{sr}\text{-}jX_{r2} = Z_r//jX_{r1}$, the current I_0 of the reader antenna coil and the coupling power P_{01c} of the reader antenna were shown as follow [30]:

$$I_0 \approx \sqrt{\frac{R_{sr}}{R_r}}\frac{U_p}{2R_{sr}}\left(1+\frac{(wM)^2}{4R_rR_t}\right)^{-1} \tag{1}$$

$$P_{01c} \approx \frac{1}{8R_t}\cdot\left|jwM\sqrt{\frac{R_{sr}}{R_r}}\frac{U_p}{2R_{sr}}\left(1+\frac{(wM)^2}{4R_rR_t}\right)^{-1}\right|^2 \tag{2}$$

where U_p was the power supply voltage of the reader; the reader antenna impedance was $Zr = R_r + jwMLr$; the tag antenna impedance $Z_{t1} = R_{t1} + jwML_{t1}$; P_{01c} was the tag chip power; M was the coupling mutual between the reader antenna coil and the tag antenna coil.

The rectification network and the matching network were composed of reactive components, as the active power was not consumed, the active power P_{01c} consumed by the tag chip was the active power P_{01l} of the load. Therefore, the tag antenna obtained the coupling power P_{01t}:

$$P_{01t} = \frac{R_t}{R_l}\cdot P_{01l} \approx \frac{R_t}{R_l}\cdot P_{01c} = \frac{U_P^2}{32R_{sr}R_rR_l} \times\cdot\left|wM\left(1+\frac{(wM)^2}{4R_rR_t}\right)^{-1}\right|^2 \tag{3}$$

For micro-strip tags, the antenna equivalent coil was coupled weakly [16], when $(wM)^2/(4R_rR_t) \ll 1$, the equation (3) can be simplified to:

$$P_{01t} = \frac{U_P^2\cdot|wM|^2}{32R_{sr}R_rR_l} \tag{4}$$

During the UHF RFID system, on the one hand, when the tags were placed close to the near field of the reader antenna, there was an inductive coupling between the reader antenna and the tag antenna, such as UHF RFID near-field application; on the other hand, when the tags were densely placed in the reading area of the reader antenna, and the tags were located in the near-field region of each other, and

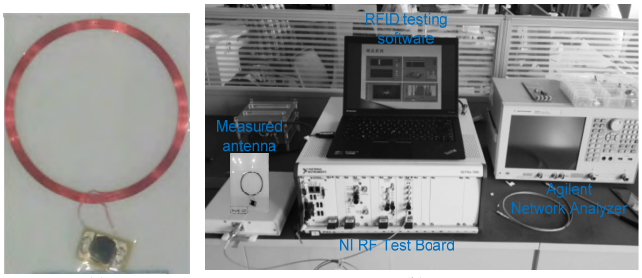

FIGURE 5. Tag's performance test instrument. (a) Antenna physical. (b) Tag performance test instrument.

there was also inductive coupling among them, which had an important influence on the transmission power and working frequency of the UHF RFID reader. When the tag space $d < 0.16\ \lambda$, the radio energy formula (4) which described the reader antenna transmitted to the working tag antenna was also applicable to the energy of the interference tag coupling to the working tag [20]. This paper assumed that when the tags were placed independently in the reader antenna identification area, all tags worked in the impedance matching state, i.e. $Z_{ti}^{*} = Z_{li}$; when the working tag was affected by the coupling of the interference tag, the working tag worked in the mismatch state. That is, when the resonant frequency of the tag antenna changed, the operating frequency of the reader antenna should also be adjusted accordingly and the operating frequency of the system will shift.

C. TEST INSTRUMENTS AND EXPERIMENTAL SCENARIOS

The type of tag antenna chip was widely used for campus card, bus deposit card and highway toll. The actual antenna was shown in Figure 5a. The experimental test platform was a VISN-R1200 radio frequency identification integrated instrument developed by Shanghai Juxing Instrument Company Ltd. (Figure 5b). The instrument contained a signal transmitting antenna and a signal acquisition antenna based on PXI vector RF module and FPGA core baseband module. It integrated self-developed radio frequency identification test software with built-in RFID protocol stack, which can transmit and collect radio frequency signals in real time. Moreover, the instrument can complete the test work under 915 MHz. In this experiment, the RF output power of the reader was 200 mW (23.01 dBm), which was greater than the activation threshold of the tag $P_{sen} = 20$ dBm. The tested tags 1 and 2 were ring tags Impinj J41 with single port connection, and the maximum read distance was 22 cm. In the experiment, the distance between the reader transmit antenna and the tag was set to a fixed value of $d_{01} = 15$ cm, and the simulation test software was ANSYS HFSS 15.0. The actual experimental scenarios during our study were shown in Figure 6. Xiao' work [31] showed that when the tags were densely placed, the coupling effect of one interference tag on the working tag was consistent with the trend of the coupling effect of multiple interference tags on the working tag, so the dual-tag systems can already reflect more performance of the tag system.

FIGURE 6. Actual experimental scene.

D. CHIPLESS UHF RFID SYSTEM

Chip RFID modulated the reflected scatter signal by controlling the load impedance of the tag antenna through the data stream stored in the chip. Chipless RFID was a new member of passive tag, it attracted people's attention because of its simple structure, printability, ultra-thin, low cost printability, and it also can work in high-temperature environments [32]. The chipless RFID contained no chip and circuit inside, but the data storing function was also completed and needed reflect information back the reader. This required a unique design of the tag structure, each tag had a slight difference in structure, chipless RFID technology produced different time domain features or spectral features by using different scatter structures. Coding to the scatter signal, each chipless tag was reflected backscattered signals with different characteristics. The backscattered signal of the tag needed to be unique and can be acquired and digitized by the reader. Unlike traditional chip RFID technology, chipless RFID technology used integrated sensor resonant structures for tag ID encoding and context awareness, which greatly reduced tag production and maintenance costs, and its unique interrogation technology also enabled the advantages of long-distance communication and simple transceiver [33].

The structure and working principle of the chipless UHF RFID system was shown in Figure 7. The operation of the chipless tag or microwave circuit loaded on the chipless RFID antenna can modulate the electromagnetic wave signal received by the antenna according to its different size and structure, so that the signal generated a specific resonant frequency and different resonant amplitude. By loading multiple radio frequency and microwave resonant circuits, multiple electromagnetic sign can be used not only as the ID of the tag, but also in the resonant circuit to integrate the sensing material for environmental sensing. Environmental parameters changed the impedance or dielectric constant of the sensing material, which in turn changed the backscattering signal of

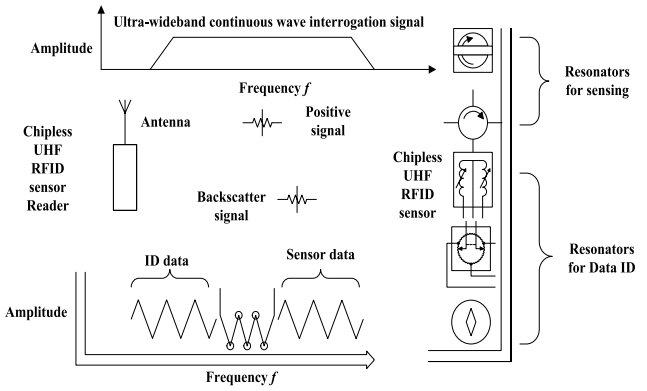

FIGURE 7. The working principle of the Chipless UHF RFID system.

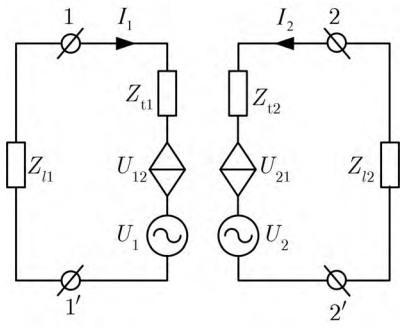

FIGURE 8. Dual-tag mutual coupling equivalent two-port network.

the antenna. The reading and accessing device realized the perception of the environment of the chipless RFID system by receiving the backscattered signal of the antenna [34]. Chipless RFID did not contain silicon chips and were highly resistant to interference, the tags required less power than traditional passive RFID tags among same operating range.

III. RELATED THEORETICAL DERIVATION

A. DERIVATION OF MUTUAL IMPEDANCE BETWEEN TAG ANTENNAS

In order to simplify the derivation process, this paper took the double tag as an example to derive the mutual impedance expression between dense tags. Figure 8 showed a dual-tag coupled equivalent two-port network in the UHF-sensing near-field region. The tag 1 was a work tag, the tag 2 was an interference tag, and the distance between tag 1 and tag 2 was d_{12}. U_1 and U_2 were the sense voltages when tag 1 and 2 placed on the near-field region of the reader antenna, respectively. I_1 and I_2 were the currents when the tag 1 and 2 worked independently. U_{12} and U_{21} were the mutual induced voltage generated between the tag 1 and tag 2. $Z_{11} = Z_{t1} + Z_{l1}$ and $Z_{12} = Z_{t2}+Z_{l2}$ were the self-impedance of the tag 1 and tag 2. Z_{12} and Z_{21} were the mutual impedance of the tag 1 and tag 2, and $U_{12} = Z_{12}I_1$, $U_{21} = Z_{21}I_2$. Then [16]:

$$\begin{bmatrix} U_1 \\ U_2 \end{bmatrix} = \begin{bmatrix} Z_{11} & Z_{12} \\ Z_{21} & Z_{22} \end{bmatrix} \begin{bmatrix} I_1 \\ I_2 \end{bmatrix} \tag{5}$$

According to formula (4), the coupling power of the tag 2 impacted on the antenna portion of the tag 1 was:

$$P_{21} \approx \frac{U_{12}^2 \cdot |wM_{21}|^2}{32R_{l2}R_{t1}R_{l1}} = \frac{(I_2\,|Z_{t2} + Z_{l2}|)^2 \cdot |wM_{21}|^2}{32R_{l2}R_{t1}R_{l1}} \tag{6}$$

The coupled active power of the tag 2 impacted on the antenna portion of the tag 1 was consumed by its antenna resistance, so P_{21} can also be expressed as:

$$P_{21} = \left(\frac{U_{21}}{|Z_{t1} + Z_{l1}|}\right)^2 \cdot R_{t1} = \left(\frac{I_2\,|Z_{21}|}{|Z_{t1} + Z_{l1}|}\right)^2 \cdot R_{t1} \tag{7}$$

Combined with formula (6), (7) can be obtained:

$$|Z_{21}| = \frac{|Z_{t1} + Z_{l1}| \cdot |Z_{t2} + Z_{l2}|}{\sqrt{32R_{t1}R_{l1}R_{t2}R_{l2}}} \cdot \omega M_{21} \tag{8}$$

where the mutual inductance M_{21} between the tag 1 antenna and the tag 2 was:

$$M_{21} = k_{21}\sqrt{L_{t1}L_{t2}} \tag{9}$$

The phase of Z_{21} was:

$$\angle(Z_{21}) = \phi_{21} \tag{10}$$

When the reader antenna senses were densely placed in the near field region with tags (number of the tags was n), and any dual-tag was located in the sensing near field region of each other, the equation (5) can be expressed:

$$\begin{bmatrix} U_1 \\ U_2 \\ \vdots \\ U_n \end{bmatrix} = \begin{bmatrix} Z_{11} & Z_{12} & \cdots & Z_{1n} \\ Z_{21} & Z_{22} & \cdots & Z_{2n} \\ \vdots & \vdots & \ddots & \vdots \\ Z_{n1} & Z_{n2} & \cdots & Z_{nn} \end{bmatrix} \begin{bmatrix} I_1 \\ I_2 \\ \vdots \\ I_n \end{bmatrix} \tag{11}$$

From the equations (9) to (11), the mutual impedance Z_{ij} between any dual-tag can be obtained:

$$\begin{cases} |Z_{ij}| = \dfrac{|Z_{ti} + Z_{li}| \cdot |Z_{tj} + Z_{lj}|}{\sqrt{32R_{ti}R_{li}R_{tj}R_{lj}}} \cdot \omega M_{ij} \quad (i, j \in N, i \neq j) \\ \angle Z_{ij} = \phi_{ij} \end{cases} \tag{12}$$

Among them, the mutual inductance between any two tag antennas was:

$$M_{ij} = k_{ij}\sqrt{L_{ti}L_{tj}} \quad (i, j \in N, i \neq j) \tag{13}$$

Among them, k_{ij} was the coupling coefficient between any dual-tag. For micro-strip tags, the coupling coefficient between the small spacer tags can be extracted by the following method.

B. COUPLING COEFFICIENT EXTRACTION METHOD IN MUTUAL IMPEDANCE

In order to facilitate the derivation of the theoretical formula, the coupling coefficient extraction between the dual-tag were taken as an example. The magnetic coupling between the equivalent circuits of the two micro-strip tag antennas can be represented by the impedance inverter K = ωL_m, as shown in Figure 9. Among them, R_{ti}, L_{ti} and C_{ti} were the equivalent

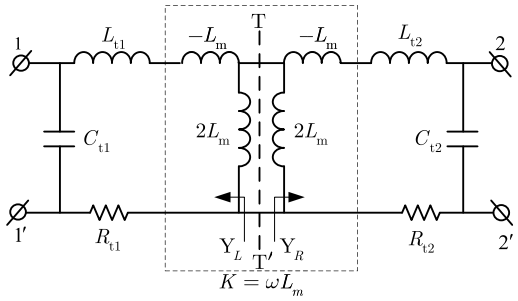

FIGURE 9. Dual-tag inductive coupling equivalent circuit.

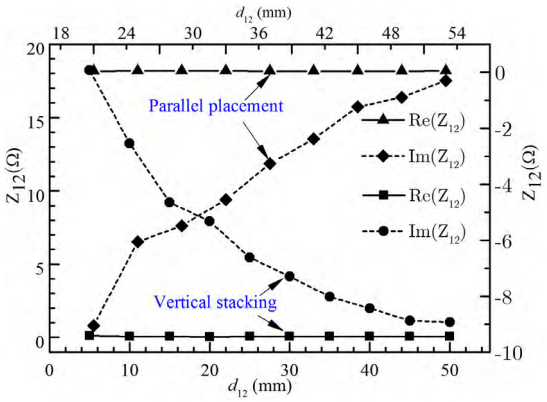

FIGURE 10. Inter-impedance simulation values between tags at different distances.

inductance, resistance, and capacitance of the micro-strip tag antenna i ($i = 1, 2$) respectively, L_m was the coupling inductance between the tag antennas. The circuit resonated condition was $Y_L = -Y_R$, that is:

$$\frac{1}{j\omega L_m} + \frac{j\omega C_{t1}}{1-\omega^2 C_{t1}(L_{t1}-L_m)} + \frac{j\omega C_{t2}}{1-\omega^2 C_{t2}(L_{t2}-L_m)} = 0 \tag{14}$$

When dual-tag types were the same, the coupling coefficient:

$$k_{12} = \frac{L_m}{\sqrt{L_{t1}L_{t2}}} = \frac{f_1^2 - f_2^2}{f_1^2 + f_2^2} \tag{15}$$

where f_1 and f_2 were the resonant frequencies (operating frequencies) of the dual-tag system, and f_1 and f_2 can be obtained by the graph of S_{12} through HFSS software. At this time, the coupling energy from the tag 2 was completely received by the tag 1, that is, $S_{12} = 0$ dB. The limitation of this method was the type of dual-tag need to be same and the space $d_{12} < 0.16\ \lambda$.

C. THE FORMULA OF THIS PAPER AND ITS COMPARISON WITH TRADITIONAL FORMULAS

As can be seen from Figure 10, the real part of the mutual impedance between the dual-tag was almost zero. When micro-strip tags were densely placed, the mutual coupling between the tags had more influence on the imaginary part of the tag antenna. Therefore, the imaginary part of the mutual

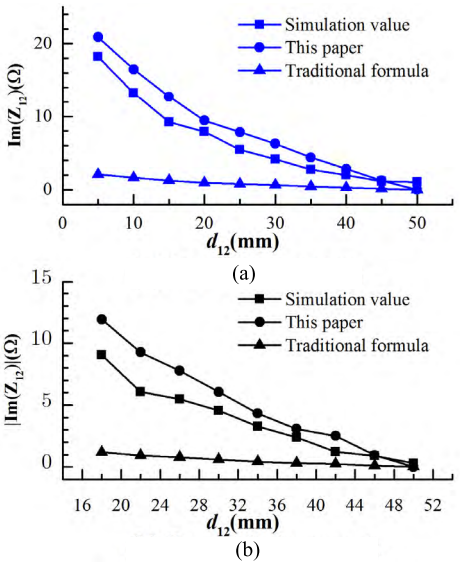

FIGURE 11. Comparison of the theoretical value of the imaginary part of the mutual impedance between the tags and the simulated value. (a) Vertical stacking. (b) Parallel placement.

impedance can reflect the mutual coupling strength between the tags.

The imaginary part of the mutual impedance between the micro-strip tag antennas was:

$$\begin{aligned} &|Im(Z_{12})| \\ &= \sqrt{|Z_{12}|^2 - |\mathrm{Re}(Z_{12})|^2} \approx |Z_{12}| \\ &= (|Z_{t1} + Z_{l1}| \cdot |Z_{t2} + Z_{l2}| / \sqrt{32R_{t1}R_{l1}R_{t2}R_{l2}}) \cdot \omega M_{12} \end{aligned} \tag{16}$$

The imaginary part of the mutual impedance between the two antenna coils in the RFID near-field system (traditional formula) was:

$$Im(Z_{12}) = wM_{12} \tag{17}$$

A correction factor was added compared formula (16) and formula (17). The values of the relevant parameters when the double tags mutually coupled were substituted into the above two formulas, and compared with the simulated values, the results were shown in Figure 11. The results showed that the average error of the formula calculated in this paper was significantly smaller than the traditional formula. As the micro-strip tag antenna was more complex and smaller than the traditional coil antenna structure. The inductive coupling between the two micro-strip tag antennas was more complicated than the inductive coupling between the two fields of the RFID near-field. Therefore, the traditional formula was no longer applicable to the mutual impedance calculation between UHF RFID near-field dense tags.

D. SYSTEM FREQUENCY SHIFT ESTIMATION METHOD CAUSED BY MUTUAL EVEN EFFECT

When there was only a single tag in the reader antenna identification area, the operating frequency of the reader depended

on the resonant frequency of the tag antenna, as known by the Thomson formula:

$$f = \frac{1}{2\pi\sqrt{L_{ti}C}} \tag{18}$$

C was composed of shunt capacitor C_p and parasitic capacitor C, i.e. $C = C_p + C'$.

Our study only considered the inductive coupling between the tags, and the capacitive coupling was not considered in the near-field region of UHF RFID, that is, the equivalent capacitance C of the tag resonant circuit was a certain value. When there were multiple tags in the antenna identification area of the reader, and the interval between the tags was small. Due to the mutual coupling between the tags, the equivalent inductance of the L_{ti} in the equation (18), that is, the resonant impedance of the working tag antenna resonant circuit was L'_{ti}, resulted the resonant frequency shift of the tag antenna, so the reader antenna should be adjusted accordingly in order to be able to identify the working tag during dense tags. Because the interference tag had random and asynchronous effects on the work tag coupling, the working tag often had multiple resonant frequency points, the lowest frequency component was the most significant, which determined the resonant frequency exhibited by the system [25]. The lowest frequency was defined as the system frequency. The traditional system frequency estimation methods included full coupling method and superposition method:

1) FULL COUPLING METHOD

The full coupling method assumed that all dual-tag antenna coils were fully coupled, i.e. $K_{ij} = 1$, at which point the resonant frequency of the tag, i.e. the system frequency was

$$f' = \frac{1}{2\pi\sqrt{L'_{ti}C_{ti}}} = \frac{1}{2\pi\sqrt{\sum_{i=1}^{n} L_{ti}C_{ti}}} \tag{19}$$

2) SUPERPOSITION METHOD

The superposition method assumed that the coupling effect of any interference tag on the working tag can be linearly superimposed, and the system frequency was:

$$f' = \frac{1}{2\pi\sqrt{L'_{ti}C_{ti}}} = \frac{1}{2\pi\sqrt{\sum_{i=1}^{n}(L_{ti} + \sum_{j=1,j\neq i}^{n} M_{ij})C_{ti}}} \tag{20}$$

Comparing equation (18) with equation (19) (20), it was easy to obtain that $f' < f$, that is, the system frequency of the tag-intensive system was shifted to the low frequency.

3) EIGENVALUE METHOD

Between dense tag antennas M_{ij} has reciprocity, so L_m in equation (14) was an n-order real symmetric positive definite matrix, so it has n eigenvalues λ_i, namely:

$$\boldsymbol{L_m X} = \lambda_i \boldsymbol{X} (i = 1, \ldots, m) \tag{21}$$

X was the eigenvector of the inductive coupling matrix.

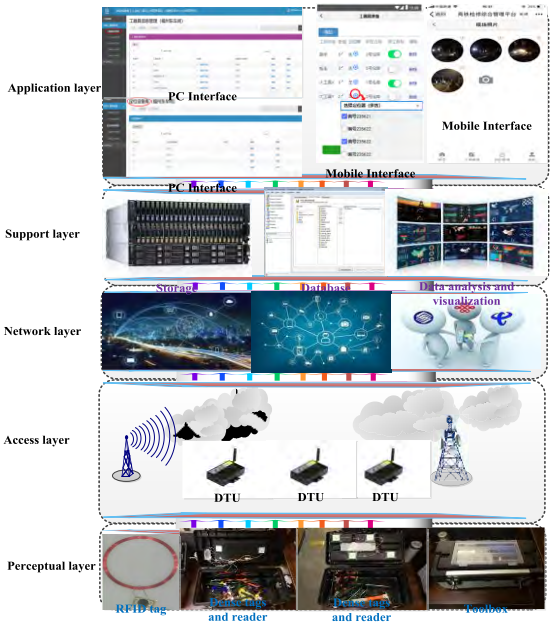

FIGURE 12. Actual IOT based monitoring systems.

In this paper, the eigenvalue λ_i of the inductive coupling matrix L_m reflected the working value of the working tag antenna in the dense tag system, which was affected by the randomness and asynchronous coupling of the remaining interference tags. Therefore, the working tag antenna in the tag dense placement system had n resonant frequencies, and correspondingly, ignoring the influence of other parameters of the system, such as the reader transmit power. The reader antenna had n transmit frequencies to activate the working tag, as mentioned above, the lowest frequency component of the system was the most significant, which reflected the overall performance of the system.

At this time, the lowest resonant frequency of the working tag antenna depended on the maximum eigenvalue of the inductance matrix L_m, that is, the system frequency was:

$$f' = \frac{1}{2\pi\sqrt{L'_{ti}C_{ti}}} = \frac{1}{2\pi\sqrt{\lambda_{\max}C}} \tag{22}$$

$$\lambda_{\max} = \mathrm{Max}[\lambda_1, \lambda_2, \cdots\cdots, \lambda_n] \tag{23}$$

As the coupling coefficient between the tag antennas $k_{ij} = M_{ij}/\sqrt{L_{ti}L_{tj}} < 1$, it can be known $0 < M_{ij} = M_{ji} < L_{ti}$ from the mutual reciprocity. The inductive coupling matrix L_m was a real symmetric matrix, which was obtained by the properties of the real symmetric matrix:

$$\mathrm{tra}(\mathbf{L}_m) = \sum_{i=1}^{n} L_{ti} = \sum_{i=1}^{n} \lambda_i \tag{24}$$

It can be seen from the above formula that the matrix L_m must have a characteristic value $\lambda_i > L_{ti}$, that is, $\lambda_{max} > L_{ti}$, which was easy to obtain that $f' < f$, the system frequency was shifted to the low frequency, which was consistent with the conclusion of the superposition method.

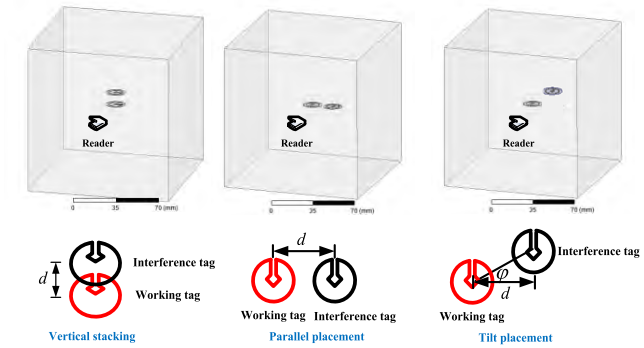

FIGURE 13. Dual-tag mutual coupling simulation model diagram.

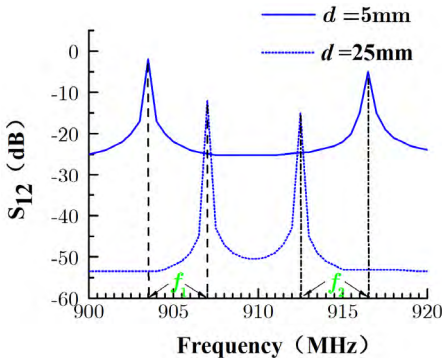

FIGURE 14. Intertag insertion loss curve (vertical overlay).

IV. EXPERIMENTS AND RESULTS

A. ACTUAL IOT BASED MONITORING SYSTEMS

Actual IOT based monitoring systems was shown in Figure 12. Power maintenance tools had complicated specifications, large quantities, and easy loss, random release, and inability to find. Based on the aforementioned multi-tags sensing theory, for the requirements of IOT applications, power maintenance tools attached with passive RFID tags were placed in the toolbox, the tag reader and power supply module were placed at the top of the toolbox based on the test requirements. The RFID-based power equipment IOT management platform mainly realized information tracking and management of construction appliances during the power maintenance process. All the tool information was entered into the system database, and the electronic tags attached to the tools were in one-to-one correspondence. The power equipment was stored in the warehouse, the warehouse can sort and query the quantity of the inventory tools and the status of the in/out status.

B. COUPLING COEFFICIENT EXTRACTION BETWEEN DUAL-TAG

In the practical application field of RFID, the intensive placement of power asset tags is randomness, at the same time, the application scenario was more complicated [11]. In this paper, two typical application scenes are set up to extract the coupling coefficient, the scene was a free space which includes a cube with side length of 120mm, which the working tag was at the center, the dual-tag mutual coupling simulation model diagram was shown in Figure 13.

When $d = 5$ mm and 25 mm, the insertion loss curve between tags is shown in Figure 14. In theory, when the dual-tag antennas are fully coupled, all the coupling energy from tag 2 is received by tag 1, that is, $S_{12} = 0$ dB; when the dual-tag antennas are weakly coupled, tag 1 received less coupling energy from tag 2, that is, $S_{12} < 20$ dB. While, during the simulation experiment, it is difficult to achieve the situation that $S_{12} = 0$ dB, so the frequency points corresponding to the two wave peaks on the S_{12} curve in Figure 14 are represented the values of f_1 and f_2. More coupling coefficient data are shown in Figure 15. As the tag spacing increases, the two resonant frequency points f_1, f_2 that in the dual-tag system

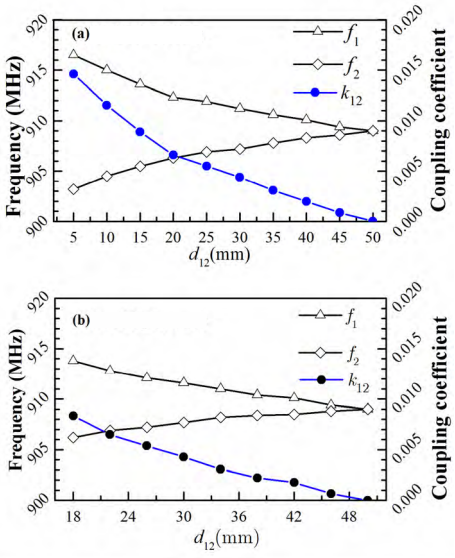

FIGURE 15. Relation between coupling coefficient and distance with different tag layouts. (a) Vertical stacking. (b) Parallel placement.

gradually approach until they converge to a frequency point. When the distance between the dual-tag exceeded a certain critical value ($< 0.16\ \lambda$), the resonance frequency point will disappear, and the coupling coefficient is nearly zero.

C. FREQUENCY SHIFT CAUSED BY MUTUAL IMPEDANCE AMONG TAGS

When tags are placed densely, the frequency of tag 1 will be shifted because of the mutual coupling from the tag 2. Taking the vertical stacking of tag as an example, when the distance d_{12} between tag 2 and tag 1 change, the working frequency can obtained when the tag is mutually coupled at different spacing during testing, which is shown in Figure 16.

Figure 16 (a), (b) are the simulation and measurement values of the echo loss S_{11} when tag 1 is affected by the coupling of tag 2 at different distances, and its optimal operating frequency (the lowest point corresponding to the S_{11} curve, abbreviated as working frequency) shifted to low frequency, which is consistent with the conclusion of reference [27]. The optimum operating frequency in Figure 16 (a), (b) is extracted and the theoretical value of the operating frequency of the

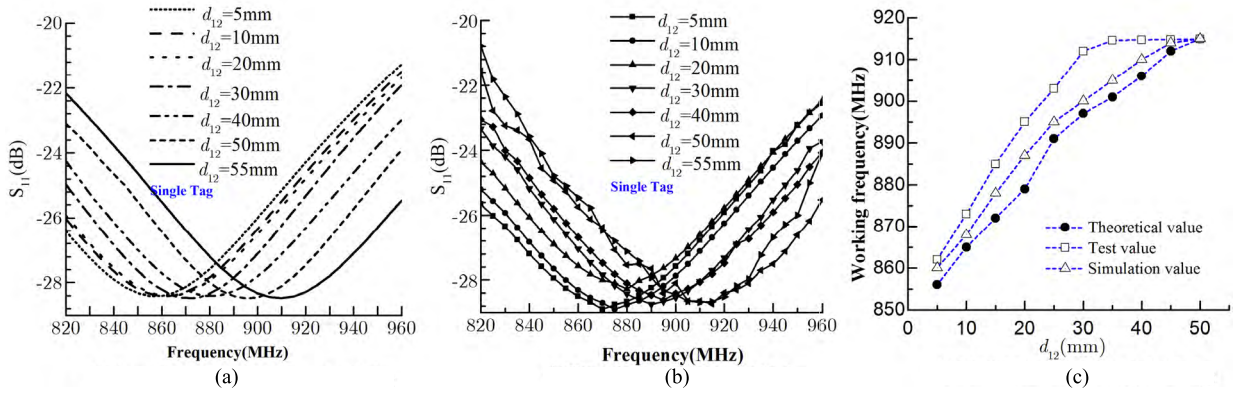

FIGURE 16. Frequency shift when tag 1 was mutually coupled. (a) Simulation value of S_{11} changed with d_{12}. (b) Test value of S_{11} changed with d_{12}. (c) Lowest point of S_{11} changed with d_{12}.

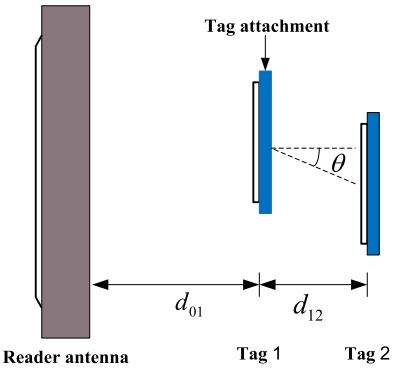

FIGURE 17. Schematic diagram of the experimental layout.

tag 1 calculated is showed in Figure 16 (c). As the electromagnetic wave generated by tag 2 antenna is more attenuated by environmental factors and the coupling effect of tag 1 to the working tag is weakened in the non-free space of the test environment. Figure 16 (c) shows that the measured frequency of tag 1 is larger than the theoretical and simulation values in the actual environment. When the tag spacing is greater than 30 mm, the mutual coupling electromagnetic wave fading between the tags became more serious, the mutual impedance between them is small, the frequency of the tag 1 is hardly shifted, and the mutual coupling effect is weak. When the spacing is less than 30 mm, the operating frequency test value of the tag 1 is close to the theoretical value calculated by the formula above, and the error is small. When the spacing is less than 30 mm, the working frequency test value of tag 1 is close to the theoretical value calculated by the formula in this paper, and the error is small. The calculation of this paper ignores the C value influences caused by the electric field coupling between the tags, so the theoretical value of the tag 1 operating frequency is smaller than the experimental measurement value and the HFSS software simulation value.

D. ANALYSIS OF INFLUENCING FACTORS OF FREQUENCY SHIFT

There are many factors affecting the mutual impedance between tags, limited to the length of the article, this paper only discusses major factors such as the relative position between tags, tag attachments, tag stacking methods. As shown in Figure 17, the distance between the working tag and the reader antenna is $d_r = 5$ cm. The distance between the working tag and the interference tag is d, and the angle between the dual-tag is θ. In the experiment, d is changed from 5 mm to 50 mm with the step value 5 mm, the angle θ changes from 0° to 60° with the step value 10°. The size of tag attachment is 8.5 cm*5.4 cm*1 mm. The tag spacing d_{12} changes from 5 mm to 50 mm with the step value 5 mm. When $d_{12} = 15$ mm, tag angle theta changes from $-75°$ to 75° with the step value 15°.

1) EFFECT OF RELATIVE POSITION ON FREQUENCY SHIFT OF WORKING TAG

Figure 18(a) shows the frequency shift change with the relative positions of the tag 2 and tag 1. When $\theta = 0°$, Δf decreases with the increase of d_{12}, but it is not a simple linear relationship. When d_{12} is smaller, the change rate of Δf is larger; when d_{12} is smaller, the change rate of Δf is smaller, and when $d_{12} > 30$ mm, there is almost unchanged. When $d_{12} = 15$ mm, the change of Δf and theta shows a symmetrical property, that is, the change of Δf in $(-75°, 0°]$ is the same as that in $[-75°, 0°)$ (as shown in Figure 18 (a), the clockwise deflection angle is positive). When θ is close to zero, Δf is larger; when θ is greater than 75°, Δf almost unchanged, at this time, the change magnetic induction line produced by tag 2 passes through tag 1 which is nearly vertical is rare, so the influence can be neglected. From the data of Figure 18 (b), the error between theoretical and experimental values is between 1.6 MHz and 7.3 MHz. When the tag spacing $d_{12} > 30$ mm and the angle $|\theta| > 60°$, the frequency shift of tag 1 is less than 13.05 MHz. For the ultra-wideband tag selected in our study, tag 2 has little influence on the mutual coupling of tag 1. Tilt placements scenario was considered for our discussion. Experimental and theoretical error under tilt placements scenario was shown in Figure 18 (c), compared with vertical and parallel placements scenario, tilt placements scenario was more complex.

2) EFFECT OF TAG ATTACHMENTS ON FREQUENCY SHIFT OF WORKING TAGS

During the simulation experiment, in order to extract the coupling coefficients between tags under different tag spacing, our study assumes that the matrix of tag antenna is similar to the object attached to it. The medium is set as FR4, Bakelite and glass, respectively. In the test, the tags are pasted on the objects of the above materials respectively, and the frequency shift of tag 1 under different materials is tested. The results are shown in Figure 19.

The simulation results in Figure 19 (a) show that for the J41 tag, when the two tags are densely placed, the coupling coefficient between them is less than 0.015. When the spacing is the same, when the label is attached to a high dielectric constant object, the coupling coefficient between the labels is low. The reason is that for microstrip labels, the low dielectric constant matrix can enhance the fringe field that produces radiation, so the electromagnetic wave fading between the dense tags is less, and the magnetic field coupling effect of the tag 2 on the tag 1 is stronger. The experimental results of Figure 19 (b)(c)(d) also show that when the label spacing is the same, when the label attachment is a high dielectric constant object, the frequency shift of the label 1 is small. As can be seen from Figure 19, the coupling coefficient between the two tags is consistent with the trend of Δf. Therefore, in the field of article-level labels, the label can be attached to a high-k dielectric object to reduce the misreading rate of the reader; in the communication between the labels, low dielectric constant attachments can be used to improve the energy utilization rate of the system, etc. It is easy to obtain from Figure 19 (b)(c)(d). When the tags are mutually coupled, the cross-resistance expression derived in this paper is significantly smaller than the traditional formula in calculating the operating frequency offset, which is more suitable for UHF. Frequency offset estimation in the near-field mutual coupling effect problem of RFID.

Figure 19 (a), when dual-tag are placed densely, the coupling coefficient between them is less than 0.015 for tags. When the distance between tags is the same, the coupling coefficient between tags is lower when tags are attached to objects with high dielectric constant. For micro-strip tags, the low dielectric constant matrix can enhance the radiation edge field, so the electromagnetic wave decay between the dense tags is less, and the magnetic field coupling effect of tag 2 to tag 1 is stronger. The experimental results of Figure 19(b) (c) (d) also show that the frequency shift of tag 1 is smaller when the tag attachment is a high dielectric constant object with the same tag spacing. From Figure 19, it can be seen that the coupling coefficients between the dual-tag are consistent with the change trend of Δf. Therefore, in the field of item-level tags, tags can be attached to high dielectric constant objects to reduce the reading error rate of readers; in the field of inter-tag communication, low dielectric constant attachments can be used to improve the energy utilization of the system. When tags are mutually coupled, the formula derived in this paper has less error than the traditional formula in calculating the frequency shift. It is more suitable for frequency shift prediction in UHF RFID near-field mutual coupling effect analysis.

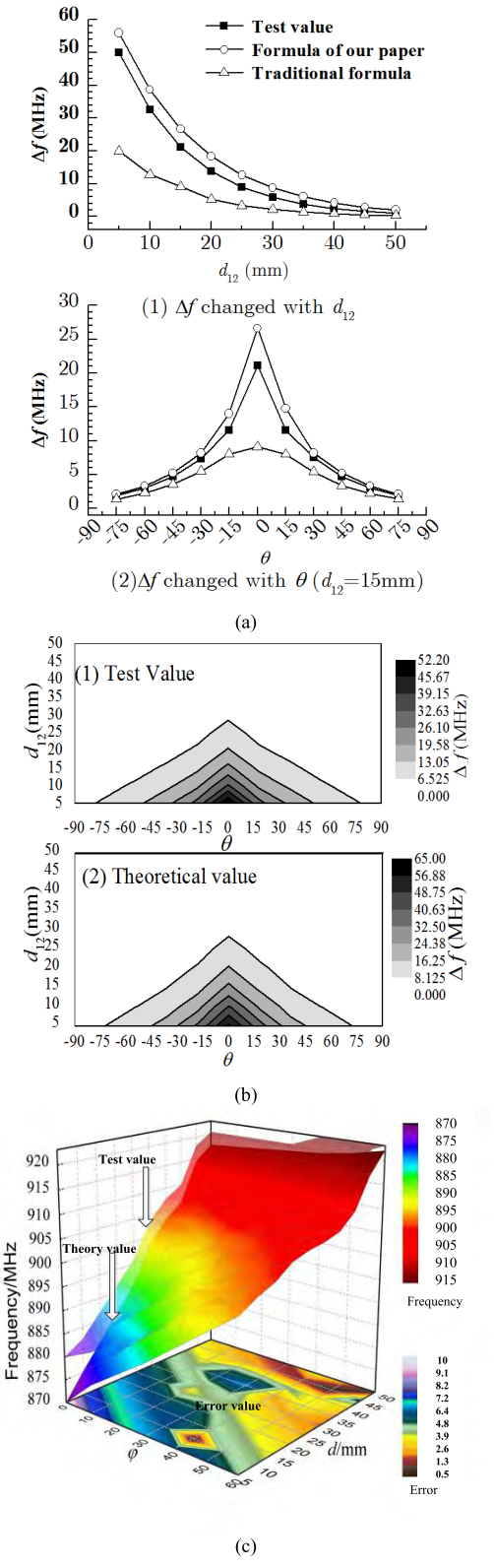

FIGURE 18. (a) Δf changed with d_{12} and θ, (b) Δf changed with relative position between tags, (c) experimental and theoretical error under Tilt placements scenario.

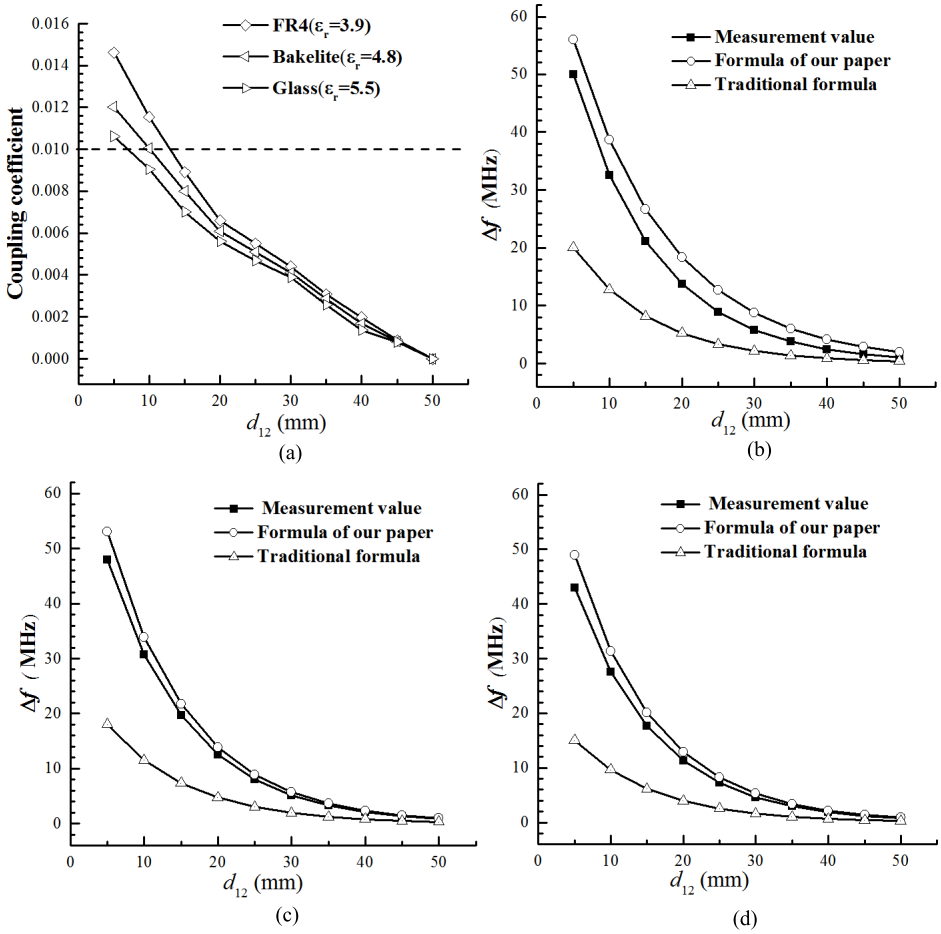

FIGURE 19. Δf changes with different medium ($\theta = 0°$). (a) Influence of material on coupling coefficient. (b) FR4. (c) Bakelite. (d) Glass.

3) SYSTEM FREQUENCY SHIFT DURING DENSE TAG MUTUAL COUPLING ENVIRONMENT

a: VERTICAL STACKING TAGS

As shown in Figure 20 (a), the UHF tag is attached to a rectangular 8.5 cm * 5.4 cm * 1 mm plate (PVC material). The number n of tags increases from 1 to 10. The spacing between any two adjacent tags is 30 mm, and the distance between the tag 10 and the reader antenna is 35 cm, which ensures that the farthest tag is still within the readable range of the reader antenna. The inductance L'_{ti} of the system and the mutual inductance M_{ij} are shown in Figure 20 (b); the operating frequency of the system is shown in Figure 20 (c).The M_{ij} correspondence principle shown in Figure 20 (b) is: $M_{|i-j|} = M_{d/5}$ $(i, j = 1, \ldots, 10; i \neq j)$. It can be seen from Figure 20(b) that as the n increases, the system inductance calculated by the full coupling method increases linearly. Obviously, this is the calculation result under ideal conditions. In practical applications, the coupling coefficient between arbitrary tags is $k_{\mathrm{ij}} < 1$; when n<7, the feature method is almost the same as the L'_{ti} calculated by the superposition method. When n>7, the L'_{ti} calculated by the feature method is smaller than the calculation result of the superposition method, and when n increases, the numerical difference will also increase. It can be seen from Figure 20 (c) that the measured value of the apparent deviation of the operating frequency of the system is calculated based on the full coupling method, which has no practical reference significance. The calculation results of the feature method and the superposition method are close to the measured values, and the calculation results of the feature method are small error and more accurate; when n>7, the calculation error of the feature method is less than 9.7%, and the calculation error of the superposition method is less than 11.8%. Therefore, the prediction result of the feature method is better than the superposition method.

b: PLANAR INTENSIVE TAGS

As shown in Figure 21, a 90 cm*90 cm*1 mm rectangular PVC plate uniformly attached with 16 UHF tags are used for the experiment. The center of the reader antenna is on the same level as the center of the PVC rectangular plate, and the spacing is set to $d_{\mathrm{r}} = 80$ cm. The space of adjacent two working tags is d, which changed from 10 cm to 20 cm, and the step value is 1 cm. The value of d changes every

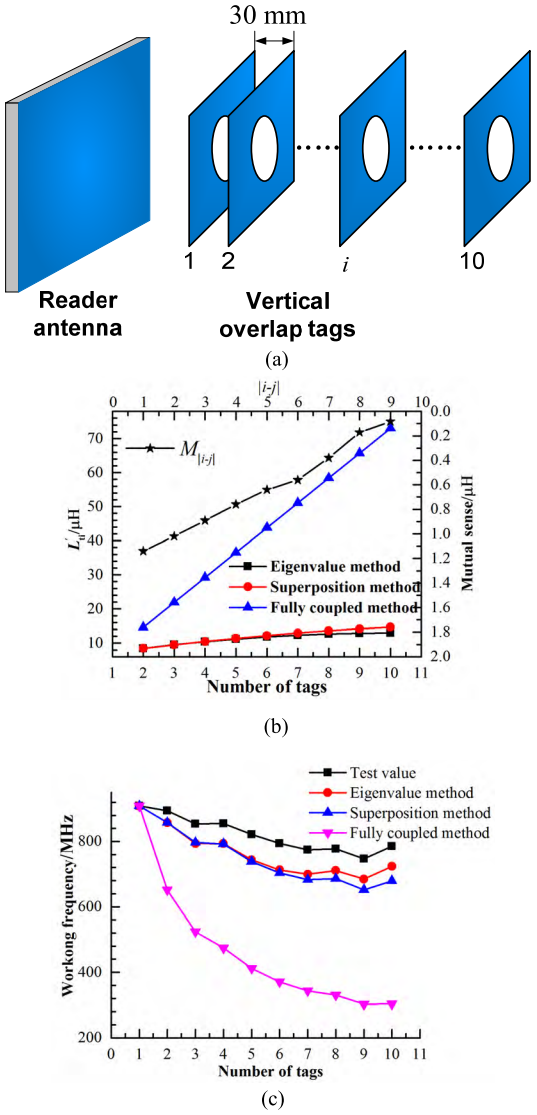

FIGURE 20. Vertical stacking tags situation. (a) Experimental schematic diagram of vertical stacking tags. (b) The inductance L'_{ti} and mutual inductance M_{ij} of n tags system. (c) The frequency of system.

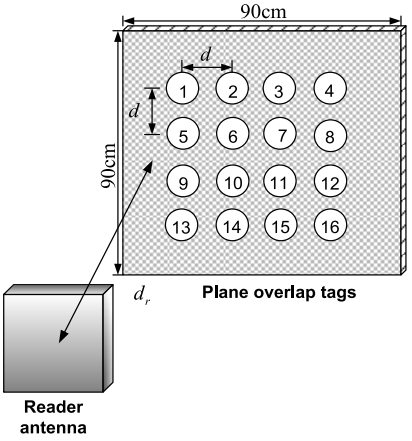

FIGURE 21. Experimental schematic diagram of planar intensive tags.

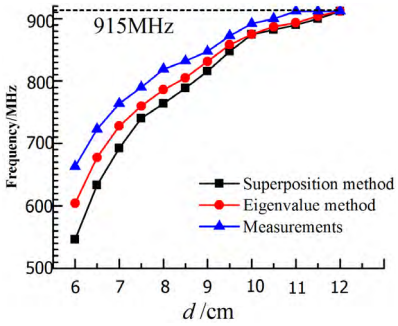

FIGURE 22. The frequency of system.

synchronization, the transmission frequency of the reader antenna adjusts until the working tag responds to the best state, that is, the return signal is clear, the operating frequency f of the system is shown in Figure 22. In this experiment, if the tag can return a signal, it is considered to be successfully read, and the recognition rate of the system is R_{ate}, which is shown in Figure 23.

In combination with the inductive coupling matrix L_{n}, the mutual inductive mutual inductivity between the planes shown in Figure 21 can correspond to a third-order matrix L_4, where $M_{12} = M_{15} = M_{51} = M_{21}$ is the average value of the mutual inductance between any two adjacent tag coils. The experimental results in Figure 22 show that the eigenvalue method for the prediction result of the system's working frequency is closer to the test quantity than the superposition method, and when the arbitrary adjacent tag spacing $d > 7$ cm, the eigenvalue method and the superposition method are almost the same, so the advantages of the method proposed in this paper lie in the estimation of small interval dense tag systems. This paper defines the system recognition rate R_{ate} as the ratio of the number of successfully read tags to the total number of tags. The experimental results in Figure 23 show that the system recognition rate is the symmetry axis of the system operating frequency curve, and the recognition rate of the system is greater than 0.875.

4) MUTUAL COUPLING EFFECT ON THE MINIMUM TRANSMIT POWER OF THE READER

The mutual coupling effect not only causes the frequency offset of the tag, but also changes the minimum transmit power of the reader antenna. As shown in Figure 24, the reader's minimum transmit power is 15 dBm when the interference tag is not present. The minimum transmit power gradually fades toward 15 dBm as the tag spacing d_{12} increases. On the other hand, when d_{12} is constant, when θ increases, minimum transmit power becomes closer to 15 dBm. The larger the deflection angle θ cause the weaker the mutual coupling effect between the tags. In practical applications, the spacing and angle of the tags should be as large as possible to reduce the transmit power of the reader. From an electromagnetic point of view, when the angle θ between the interference tag and the work tag is 90°, the effective area of the magnetic field

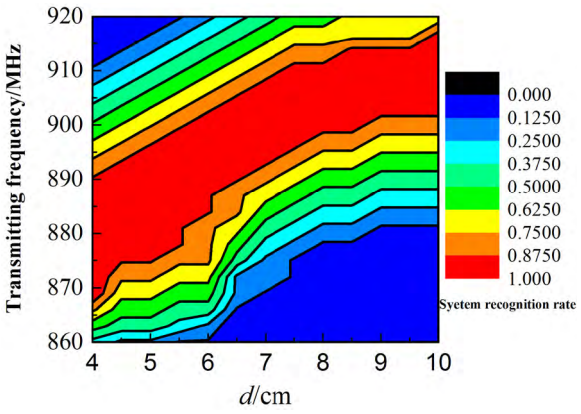

FIGURE 23. The rate of system recognition varies with space d and the transmitter frequency.

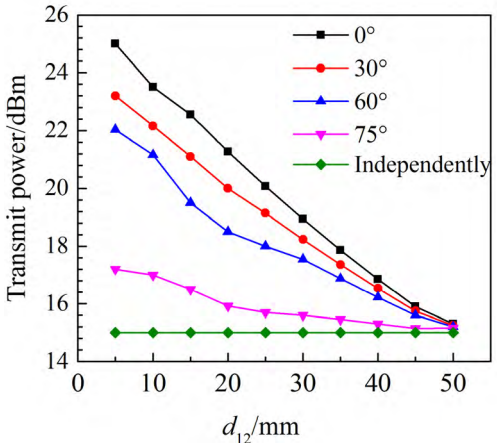

FIGURE 24. The minimum transmit power changes with d_{12} and θ.

line generated from the interference tag through the work tag is nearly zero.

V. CONCLUSION

The estimation of the frequency of the dense tag system helps to adjust the transmit power and transmission frequency of the reader antenna and to improve the recognition rate of the system. Based on the transformer model, this paper derived the mutual impedance expression between the inductively coupled dual tags densely placed in the UHF RFID sensing near-field region from the perspective of wireless energy transmission. The inductive coupling type tag J41 was taken as an example to simulate, it is verified by experiments that the transimpedance expression is more suitable for pre-resonance problem of the frequency shift, which estimated research in the mutual coupling effect between inductively coupled double-loop tag antennas in UHF RFID near-field systems when $d_{12} < 30$ mm, and it has small error and high accuracy. When the densely placed tag type was determined, the coupling coefficient between the tags only affected the mutual impedance. The error range between the theoretical value of Δf and the experimental value was (1.6 MHz∼7.3 MHz), and when the tag spacing $d_{12} > 30$ mm, the angle $|\theta| > 60°$, the frequency shift of the working tag was less than about 13.05 MHz; Δf was negatively correlated with the dielectric constant of the tag attachment. For a vertically stacked dense tag scene, when the number of tags $n > 7$, the eigenvalue method estimation error was less than 9.8%, and within a certain range, the larger n was, the higher the estimation accuracy of the eigenvalue method was. When the transmit frequency of the reader antenna was within a 50 MHz bandwidth centered on the system frequency, the recognition rate of the system was as high as 87.5%. The research results have guiding significance for the rapid identification and location of power assets under dense RFID tag environment.

REFERENCES

[1] N. Kshetri, "The evolution of the Internet of Things industry and market in China: An interplay of institutions, demands and supply," *Telecommun. Policy*, vol. 41, no. 1, pp. 49–67, Feb. 2017.
[2] C. A. Tokognon, B. Gao, G. Y. Tian, and Y. Yan, "Structural health monitoring framework based on Internet of Things: A survey," *IEEE Internet Things J.*, vol. 4, no. 3, pp. 619–635, Jun. 2017.
[3] M. E. S. Saeed, Q.-Y. Liu, G. Y. Tian, B. Gao, and F. Li, "AKAIoTs: Authenticated key agreement for Internet of Things," *Wireless Netw.*, vol. 25, no. 6, pp. 3081–3101, Mar. 2018.
[4] P. Solic, J. Radic, and N. Rozic, "Software defined radio based implementation of RFID tag in next generation mobiles," *IEEE Trans. Consum. Electron.*, vol. 58, no. 3, pp. 1051–1055, Aug. 2012.
[5] A. Hassan, H. Bruining, T. Musa, and M. Chahardowli, "The use of RFID technology to measure the compositions of diethyl ether-oil-brine mixtures in enhanced imbibition experiments," *J. Petroleum Sci. Eng.*, vol. 156, pp. 769–779, Jul. 2017.
[6] L. Catarinucci, D. De Donno, and R. Colella, "A cost-effective SDR platform for performance characterization of RFID tags," *IEEE Trans. Instrum. Meas.*, vol. 61, no. 4, pp. 903–911, Dec. 2012.
[7] J. Choi, I. Y. Lee, K. Lee, S. O. Yun, J. Kim, J. Ko, G. Yoon, and S. G. Lee, "A 5.8-GHz DSRC transceiver with a 10 μA interference-aware wake-up receiver for the Chinese ETCS," *IEEE Trans. Microw. Theory Techn.*, vol. 62, no. 12, pp. 3146–3160, Sep. 2014.
[8] A. Karttunen, A. F. Molisch, S. Hur, J. Park, and C. J. Zhang, "Spatially consistent street-by-street path loss model for 28-GHz channels in micro cell urban environments," *IEEE Trans. Wireless Commun.*, vol. 16, no. 11, pp. 7538–7550, Nov. 2017.
[9] E. Perret, "Displacement sensor based on radar cross-polarization measurements," *IEEE Trans. Microw. Theory Techn.*, vol. 65, no. 3, pp. 955–966, Mar. 2017.
[10] H. Ma, W. Yi, K. Wang, and Z. Ma, "The optimization for hyperbolic positioning of UHF passive RFID tags," *IEEE Trans. Autom. Sci. Eng.*, vol. 14, no. 4, pp. 1590–1600, Oct. 2017.
[11] A. Michel, P. Nepa, X. Qing, and Z. N. Chen, "Considering high-performance near-field reader antennas: Comparisons of proposed antenna layouts for ultrahigh-frequency near-field radio-frequency identification," *IEEE Antennas Propag. Mag.*, vol. 60, no. 1, pp. 14–26, Feb. 2018.
[12] M. Omer and G. Y. Tian, "Indoor distance estimation for passive UHF RFID tag based on RSSI and RCS," *Measurement*, vol. 127, pp. 425–430, Oct. 2018.
[13] J. Zhang and G. Y. Tian, "UHF RFID tag antenna-based sensing for corrosion detection & characterization using principal component analysis," *IEEE Trans. Antennas Propag.*, vol. 64, no. 10, pp. 4405–4414, Oct. 2016.
[14] K. Jaakkola, H. Sandberg, M. Lahti, and V. Ermolov, "Near-field UHF RFID transponder with a screen-printed graphene antenna," *IEEE Trans. Compon., Packag., Manuf. Technol.*, vol. 9, no. 4, pp. 616–623, Feb. 2019.
[15] Y. Yao, C. Cui, J. Yu, and X. Chen, "A meander line UHF RFID reader antenna for near-field applications," *IEEE Trans. Antennas Propag.*, vol. 65, no. 1, pp. 82–91, Jan. 2017.
[16] Y. Yao, Y. Liang, J. Yu, and X. Chen, "Design of a multipolarized RFID reader antenna for UHF near-field applications," *IEEE Trans. Antennas Propag.*, vol. 65, no. 7, pp. 3344–3351, May 2017.
[17] F. Xiao, Z. Wang, N. Ye, R. Wang, and X.-Y. Li, "One more tag enables fine-grained RFID localization and tracking," *IEEE/ACM Trans. Netw.*, vol. 26, no. 1, pp. 161–174, Feb. 2018.

[18] Z. Q. Wang, F. Xiao, N. Ye, R. C. Wang, and P. L. Yang, "A see-through-wall system for device-free human motion sensing based on battery-free RFID," *ACM Trans. Embedded Comput. Syst.*, vol. 17, no. 1, pp. 1–21, Sep. 2017.
[19] J. K. Pakkathillam and M. Kanagasabai, "A novel UHF near-field RFID reader antenna deploying csrr elements," *IEEE Trans. Antennas Propag.*, vol. 65, no. 4, pp. 2047–2050, Apr. 2017.
[20] L. Zuo, Y. G. He, B. Li, Y. Q. Zhu, and G. F. Feng, "Theory and measurement for mutual coupling effect of ultra high frequency radio-frequency identification in dense environments," *Acta Phys. Sinica*, vol. 62, no. 4, pp. 1021–1029, Apr. 2013.
[21] Z.-Y. Peng, X.-F. Ren, C.-Y. Meng, and S. Li, "Study on gain characteristics of dual ultra-high-frequency radio frequency identification tag antennas with small interval," *J. Electron. Inf.*, vol. 37, no. 7, pp. 1874–1878, Jul. 2015.
[22] Z. Y. Peng, C. Y. Meng, and X. F. Ren, "Design method of tag mutual resistance in dense environment," *J. Electron. Inf.*, vol. 37, no. 6, pp. 1304–1309, Jun. 2015.
[23] A. I. Sunny, G. Y. Tian, and J. J. Zhang, "Low frequency (LF) RFID sensors and selective transient feature extraction for corrosion characterisation," *Sens. Actuators A, Phys.*, vol. 241, pp. 34–43, Apr. 2016.
[24] J. Han, C. Qian, X. Wang, D. Ma, J. Z. Zhao, P. F. Zhang, W. Xi, and Z. P. Jiang, "Twins: Device-free object tracking using passive tags," *IEEE/ACM Trans. Netw.*, vol. 24, no. 3, pp. 1605–1617, Jun. 2016.
[25] J. R. Xu and S. R. Qian, "The design of high frequency RFID overlapping label carrier frequency conversion device," *Comput. Eng.*, vol. 40, no. 2, pp. 317–320, Feb. 2014.
[26] S. Sajal, B. D. Braaten, V. Marinov, O. Swenson, and Y. Atanasov, "A low-cost compact antenna design on a paper substrate for near-field passive UHF RFID tags," *Microw. Opt. Technol. Lett.*, vol. 59, no. 5, pp. 1052–1056, May 2017.
[27] Z. Y. Peng, X. F. Ren, C. Y. Meng, S. Li, and W. T. Chen, "Study on frequency shift characteristics of mutual coupling between UHF RFID tags in dense environment," *Electron. Meas. Technol.*, vol. 38, no. 6, pp. 11–15, Jun. 2015.
[28] H. L. Zhu, X. Z. Lai, H. Y. Dai, and S. L. Lai, "Effects of metal environment on HF frequency band RFID system," *J. South China Univ. Technol. (Natural Sci. Ed.)*, vol. 36, no. 5, pp. 84–88, May 2008.
[29] X. Qing and Z. N. Chen, "Proximity effects of metallic environments on high frequency RFID reader antenna: Study and applications," *IEEE Trans. Antennas Propag.*, vol. 55, no. 11, pp. 3105–3111, Nov. 2007.
[30] B. Jiang, J. R. Smith, M. Philipose, S. Roy, K. Sundara-Rajan, and A. V. Mamishev, "Energy scavenging for inductively coupled passive RFID systems," *IEEE Trans. Instrum. Meas.*, vol. 56, no. 1, pp. 118–125, Feb. 2007.
[31] F. X. Xiao, X. G. Zhang, and S. Li, "RFID tags constrained links in a densely distributed environment," *J. Shanghai Univ. (Natural Sci.)*, vol. 5, pp. 624–632, Oct. 2014.
[32] A. M. J. Marindra and G. Y. Tian, "Chipless RFID sensor tag for metal crack detection and characterization," *IEEE Trans. Microw. Theory Techn.*, vol. 66, no. 5, pp. 2452–2462, May 2018.
[33] S. Dey, J. K. Saha, and N. C. Karmakar, "Smart sensing: Chipless RFID solutions for the Internet of everything," *IEEE Microw. Mag.*, vol. 16, no. 10, pp. 26–39, Nov. 2015.
[34] E. M. Amin, J. K. Saha, and N. C. Karmakar, "Smart sensing materials for low-cost chipless RFID sensor," *IEEE Sensors J.*, vol. 14, no. 7, pp. 2198–2207, Jul. 2014.

GUOLONG SHI received the B.S. degree from Hohai University, Nanjing, China, in 2010, and the M.Sc. degree from the University of Science and Technology of China, Hefei, Anhui, in 2013. He is currently pursuing the Ph.D. degree with the Hefei University of Technology, Hefei. His research interests mainly include wireless sensor networks, intelligent sensor signal processing, computer software, and pattern recognition algorithm.

YIGANG HE received the M.Sc. degree in electrical engineering from Hunan University, in 1992, and the Ph.D. degree from Xi'an Jiaotong University, in 1996. He is currently a Professor and the Head of the School of Electrical Engineering and Automation, Hefei University of Technology. His research interests include circuit theory and its applications, testing and fault diagnosis of analog and mixed-signal circuits, smart grid, radio-frequency identification technology, and intelligent signal processing. He is one of the winners of the National Distinguished Young Scientists Foundation.

BAIQIANG YIN received the M.Sc. degree in electrical engineering from Nanhua University, Hengyang, China, in 2008, and the Ph.D. degree in electrical engineering from Hunan University, Hunan, China, in 2014. He joined the Hefei University of Technology, China, where he is currently an Assistant Professor with the School of Electrical and Automation Engineering. His teaching and research interests include the testing and fault diagnosis of analog and mixed-signal circuits, electrical signal detection, radio-frequency identification technology, and intelligent signal processing. He has published some 20 journal and conference papers in the aforementioned areas.

LEI ZUO received the B.E., M.E., and Ph.D. degrees in electrical engineering from Hunan University, Changsha, China, in 2005, 2009, and 2013, respectively. He joined the School of Electrical and Automation Engineering, Hefei University of Technology, Hefei, China, in 2013. His research interests include radio-frequency identification technology, wireless sensor networks, signal processing, and neural network algorithm. He has published some ten journal and conference papers in the RFID areas.

PEILIANG SHE received the B.Sc. degree from the Anhui University of Science and Technology, in 2016. He is currently pursuing the M.Sc. degree with the Hefei University of Technology. His main research interests include RFID technology, and tag IC design and testing.

WENBO ZENG received the B.S. degree from Hunan University, Changsha, China, in 2016. He is currently pursuing the Ph.D. degree with the Hefei University of Technology, Hefei, Anhui. His research interests mainly include wireless communication channel modeling, key technologies for wireless sensor, and wireless communication testing in smart grids.

FARHAN ALI received the B.S. degree in electronics and communication and the M.S. degree in electrical and electronics systems (engineering) from the University of Lahore, Pakistan, in 2012 and 2016, respectively. He is currently pursuing the Ph.D. degree in electrical engineering and automation with the Hefei University of Technology, Hefei, China. His research interests include wireless communication, 5G, and the Internet of Things.